Copper insertion facilitates water-soluble porphyrin binding to rA·rU and rA·dT base pairs in duplex RNA and RNA·DNA hybrids

ARTICLE *in* BIOCHEMISTRY · NOVEMBER 2002

Impact Factor: 3.02 · DOI: 10.1021/bi026139z · Source: PubMed

6 AUTHORS, INCLUDING:

Yoshinobu Ishikawa
University of Shizuoka

80 PUBLICATIONS **548** CITATIONS

SEE PROFILE

Copper Insertion Facilitates Water-Soluble Porphyrin Binding to rA·rU and rA·dT Base Pairs in Duplex RNA and RNA·DNA Hybrids†

Tadayuki Uno,* Katsumasa Aoki, Tomoko Shikimi, Yumi Hiranuma, Yoshikazu Tomisugi, and Yoshinobu Ishikawa

Faculty of Pharmaceutical Sciences, Kumamoto University, Oehonmachi, Kumamoto 862-0973, Japan

Received May 15, 2002; Revised Manuscript Received August 1, 2002

ABSTRACT: The binding of the copper(II) complex of water-soluble *meso*-tetrakis(*N*-methylpyridinium-4-yl)porphyrin (TMPyP) to double-helical polynucleotides has been studied by optical absorption, circular dichroism (CD), and resonance Raman spectroscopic methods. The target polymers were RNA and RNA·DNA hybrids consisting of rA·rU, rI·rC, rA·dT, and rI·dC base pairs. Relative to the metal-free H_2TMPyP [Uno, T., Hamasaki, K., Tanigawa, M., and Shimabayashi, S. (1997) *Inorg. Chem. 36,* 1676−1683], CuTMPyP binds to poly(rA)·poly(dT) and poly(rA)·poly(rU) with a greatly increased binding constant. The external self-stacking of the porphyrin on the surface of the polymers was evident from the strong conservative-type induced CD signals. The signal intensity correlated almost linearly with the number of stacking sites on the polymer except for poly(rA)·poly(dT), which showed extraordinarily strong CD signals. Thus, the bound porphyrin may impose an ordered architecture on the polymer surface, the stacking being facilitated by the more planar nature of the CuTMPyP than the nonmetal counterpart. Resonance Raman spectra of the stacked CuTMPyP were indistinguishable from those of the intercalated one with positive δ(Cβ−H) and negative δ(Cm−Py) bending shifts, and hence the stacked porphyrins are suggested to adopt a similar structure to that of intercalated ones. Porphyrin flattening by copper insertion opens a new avenue for medical applications of porphyrins, blocking biological events related to RNA and hybrids in malignant cells.

The water-soluble tetracationic porphyrin *meso*-tetrakis(*N*-methylpyridinium-4-yl)porphyrin (TMPyP)[1] has been under intensive study with special interest in its potential therapeutic use. H_2TMPyP (Chart 1) has many favorable properties for photodynamic therapy (*1*) and causes damage to DNA in tumor cells upon irradiation, leading to cell death (*2*). H_2TMPyP causes the production of singlet oxygen with high quantum yield (*3*), and production of the singlet oxygen linearly correlates with the photonuclease activity of cationic porphyrins (*4*).

Three modes of cationic porphyrin binding to double helical DNA have been proposed: intercalation, outside groove binding, and outside binding with self-stacking of the porphyrins (*5*-*7*). The binding modes are affected by the DNA sequence as well as the solvent composition. H_2TMPyP binds 5′-CG sequences predominantly through intercalation, whereas AT rich sequences favor outside groove binding with binding constants comparable to those for intercalation (*8*, *9*). Increasing the ionic strength occasionally promotes long-range aggregates on the nucleic acid polymer, resulting in a helical alignment of porphyrin on the polymer surface (*10*, *11*). The sign of the induced CD spectrum of porphyrins bound to nucleic acids provides a convenient signature for the mode of binding to DNA (*9*, *12*): a positive induced CD band in the Soret region is indicative of groove binding, while a negative induced CD band indicates intercalation. Some porphyrins produce intense bisignate CD spectra whose profile reveals the helical sense of the DNA. The helical alignment of the porphyrin transition dipoles gives rise to the very large, conservative CD signals (*10*, *13*).

Chart 1: Chemical Structure of H_2TMPyP (Left) and CuTMPyP (Right)

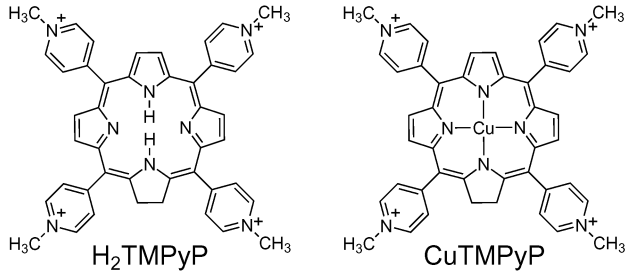

Recently, the interactions between H_2TMPyP and four-stranded DNA structures (quadruplexes or tetraplexes) by guanine-rich DNA oligomers have generated considerable interest (*14*−*20*). Tandemly repeating guanine clusters occur at the 3′ ends of chromosomal DNA (*21*−*23*), and stabilization of this unique structure is believed to impede access of DNA telomerase to its substrate DNA. DNA telomerase has recently been linked to the longevity of many cancer cells, and the processivity of this enzyme may be critical for the immortalization and proliferative potential of these cells (*24*, *25*).

† This work is supported by a grant for Science Research (13557199 to T. U.) from the Japan Society for Promotion of Science.

* Corresponding author. Telephone and Fax: +81-96-371-4350. E-mail: unot@gpo.kumamoto-u.ac.jp.

[1] Abbreviations: TMPyP, *meso*-tetrakis(*N*-methylpyridinium-4-yl)-porphyrin; CD, circular dichroism.

10.1021/bi026139z CCC: $22.00
Published on Web 10/05/2002

H_2TMPyP can interact not only with double helical and four-stranded DNA (*26*), but also with duplex RNA (*27*). RNA·DNA hybrid structures are an attractive target for a new type of cancer chemotherapy (*28*) since the hybrid structures play key roles in many biological processes. RNA·DNA hybrids are transiently formed in the course of DNA replication (*29*), telomere replication by telomerase (*30*), and the replication of retroviruses by reverse transcription (*29*), and the rate of replication is often elevated in malignant cells. Inhibition of telomerase was attempted by using RNA or DNA oligonucleotides to block the formation of the RNA·DNA hybrid structure that normally initiates telomere replication (*31*). Bisdistamycins were explored as selective binding agents to a model Okazaki fragment containing both DNA duplex and RNA·DNA hybrid regions (*32*, *33*).

Recently, molecules have been discovered which have a high affinity for RNA·DNA hybrids, as revealed by a competition dialysis assay (*34*). Ellipticine, ethidium, coralyne, propidium, and TAS103 bind preferentially to the poly(rA)·poly(dT) hybrids. These drugs share a common structural motif having a planar aromatic ring system with a "bay" region. Although H_2TMPyP was also investigated, its binding affinity was reported to be modest (*34*). Since TMPyP shares a similar chemical motif to H_2TMPyP and indeed binds to DNA with high affinity, we focused on enhancing the binding properties of TMPyP. Previously we have measured the binding of metal-free H_2TMPyP to RNA and RNA·DNA hybrids (*35*), and in the present study, we observed that copper(II) insertion into the porphyrin macrocycle greatly enhances binding to duplexes having rA·rU and rA·dT base pairs. The high affinity was attributed to the planar nature of CuTMPyP (Chart 1), as will be revealed by various spectroscopic methods. Since the CuTMPyP was found to bind with self-stacking on the polymer surface sequestering the base pairs, the simple copper insertion exploits a new field for medical applications of porphyrins, blocking biological events related to RNA and hybrids in malignant cells.

MATERIALS AND METHODS

Materials. The tosylate salt of H_2TMPyP was purchased from Dojin Chemical Co., and the copper(II) derivative was prepared using published methods (*36*, *37*). The stock solution of CuTMPyP in water was passed through a 0.45 μm filter, and the concentration of the porphyrin was determined from the molar absorptivity at the Soret maximum (231 mM^{-1} cm^{-1} at 424 nm) (*36*). The single-strand homopolymers poly(rA), poly(rU), and poly(dT) were purchased from Sigma, while poly(rI), poly(rC), and poly(dC) were from Pharmacia. The nucleotide concentrations were determined from the appropriate molar absorptivities as reported (*35*). The duplexes were prepared in solutions containing 10 mM sodium phosphate, 1 mM EDTA, and 0.1 M sodium chloride (pH 7.0) by mixing the appropriate single strands in a 1:1 molar ratio. This solution was heated to 95 °C for 10 min and then cooled slowly to room temperature to minimize formation of competing secondary structures. The concentrations of the duplexes were expressed in terms of base pairs.

Spectral Measurements. Aliquots of duplex solutions were added to the solution of CuTMPyP (ca. 5 μM), and absorption spectra were recorded with a Beckman DU640 spectrophotometer at 25 °C. The induced CD spectra of CuTMPyP (ca. 5 μM) were measured at selected concentrations of the duplexes, and 20 independent spectra were averaged. Conversely, aliquots of the CuTMPyP solution were added to a solution of the duplexes (ca. 30 μM), and four independent CD spectra in the UV range were averaged. The CD spectra were recorded with a Jasco J-600 spectropolarimeter, and all spectra were baseline corrected and smoothed. All the spectral measurements were made in a buffer containing 10 mM sodium phosphate, 1 mM EDTA, and 0.1 M sodium chloride (pH 7.0). The binding constants (K) and the number of binding sites per base pair (n) were estimated from the spectral changes, according to Scatchard analysis (*38*). In brief, the absorbance changes were analyzed using an equation:

$$[B]_0/(1 - \alpha) = (1/Kn)(1/\alpha) + [P]_0/n$$

where $[B]_0$ and $[P]_0$ are the total concentrations of the base pairs and the porphyrin, respectively. The mole fraction of free porphyrin, α, can be determined by

$$\alpha = (A - A_f)/(A_i - A_f)$$

where A denotes absorbance at a proper wavelength and A_i and A_f denote that at the initial and final stages, respectively.

Resonance Raman spectra were recorded on a Jasco double monochromator (R-800) using a Kimmon IK4121R-G He−Cd laser (441.6 nm) with a laser power of 35 mW at the sample. A spinning Raman cell was used to minimize sample decomposition. The samples contained ca. 5 μM CuTMPyP in 10 mM sodium phosphate, 1 mM EDTA, and 0.1 M sodium chloride (pH 7.0). Thus, the absorption, induced CD, and resonance Raman spectra of CuTMPyP were measured under nearly identical conditions.

We also tried to measure CuTMPyP binding to poly(rG)·poly(rC) and poly(rG)·poly(dC), but fiber precipitation within a few minutes was observed. Since the fiber was red, CuTMPyP must have contributed to fiber formation, and we did not examine either polymer further.

RESULTS

Absorption Spectroscopy. The change in the absorption spectrum of CuTMPyP upon addition of poly(rA)·poly(rU), poly(rA)·poly(dT), poly(rI)·poly(rC), and poly(rI)·poly(dC) duplexes is shown in Figure 1. In every case, a single set of isosbestic points was observed, indicating that binding is a one step process. The Soret maximum shifted commonly to a longer wavelength (about 10 nm) and showed a large hypochromicity (about 30%). These spectral features were exhibited by all the duplexes examined, the absorption spectral changes caused by the CuTMPyP being indistinguishable for the RNA duplexes and the hybrids. The bathochromic shift was modest compared with that for metal-free H_2TMPyP (*35*), where the Soret maximum was red-shifted by about 15 nm (Table 1). The large hypochromicity suggested that the porphyrin π electrons were perturbed considerably upon binding to the duplexes.

Plots of the absorbance changes at the Soret maximum (424 nm) versus the concentration of base pairs are shown in Figure 2. It is clear that porphyrin binding to poly(rI)·

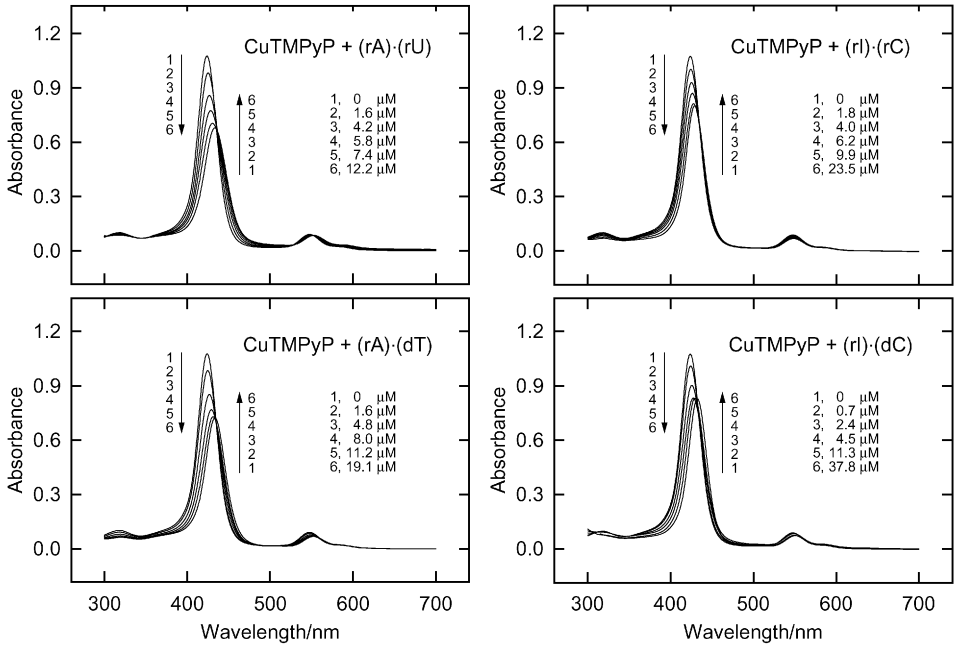

FIGURE 1: Absorption spectral change of CuTMPyP on the addition of duplexes. The porphyrin concentration was 4.66 μM. The spectra were recorded in 10 mM sodium phosphate, 1 mM EDTA, 0.1 M NaCl (pH 7.0). Top left, concentrations of poly(rA)·poly(rU) were as follows: 1, 0 μM; 2, 1.6 μM; 3, 4.2 μM; 4, 5.8 μM; 5, 7.4 μM; 6, 12.2 μM. Bottom left, concentrations of poly(rA)·poly(dT) were as follows: 1, 0 μM; 2, 1.6 μM; 3, 4.8 μM; 4, 8.0 μM; 5, 11.2 μM; 6, 19.1 μM. Top right, concentrations of poly(rI)·poly(rC) were as follows: 1, 0 μM; 2, 1.8 μM; 3, 4.0 μM; 4, 6.2 μM; 5, 9.9 μM; 6, 23.5 μM. Bottom right, concentrations of poly(rI)·poly(dC) were as follows: 1, 0 μM; 2, 0.7 μM; 3, 2.4 μM; 4, 4.5 μM; 5, 11.3 μM; 6, 37.8 μM.

Table 1: Spectral Comparison between H_2TMPyP and CuTMPyP Bound to the Duplexes

duplexes	metal	$\Delta\lambda$/nm[a]	H/%[b]	induced CD/nm[c]	
poly(rA)·poly(rU)	Cu	+9	37	411 (+10.5)	430 (−14.4)
	H_2[d]	+16	39	423 (+1.9)	441 (−4.7)
poly(rA)·poly(dT)	Cu	+10	33	422 (+23.8)	440 (−55.9)
	H_2[d]	+16	38		439 (−5.5)
poly(rI)·poly(rC)	Cu	+5	25	411 (+10.2)	432 (−15.5)
	H_2[d]	+11	46	421 (+5.0)	444 (−9.3)
poly(rI)·poly(dC)	Cu	+8	23		427 (−2.9)
				414 (+25.2)	430 (−29.6)
	H_2[d]	+15	39		439 (−6.1)
				423 (+8.8)	443 (−20.4)

[a] Bathochromic shift. [b] The hypochromicity (H/%) was determined by the equation $H = (\epsilon_f - \epsilon_b)/\epsilon_f \times 100$, where ϵ_f and ϵ_b represent the molar absorptivities of free and bound porphyrins, respectively, which were determined at the respective Soret maxima. [c] Induced CD peaks. The values in parentheses are molar ellipticities ($[\theta]/10^4$ deg cm^2 dmol^{-1}). [d] From ref *35*.

poly(dC) is a two-step process, although other duplexes showed a single binding step. Since isosbestic points were observed (Figure 1), the two porphyrin species produced upon binding to poly(rI)·poly(dC) must exhibit quite similar absorption spectra, and hence the electronic structure of the two products must be nearly the same. For other duplexes, the binding process could be analyzed by a simple equilibrium process, and the binding constant (K) and the number of binding sites on the duplex (n_{AB}) were determined from the absorbance changes. The values of K and n_{AB} thus obtained are summarized in Table 2. Theoretical curves with these values were drawn in Figure 2 and were found to fit nicely to the absorbance changes actually observed. In the case of poly(rI)·poly(dC), the binding process was complex and Scatchard analysis was not possible. In turn, the number of binding sites was estimated from the break points (indicated by arrows in Figure 2) to be 0.19 and 1.17. Comparing these parameters with those for H_2TMPyP, it is clear that the n_{AB} values are generally small for CuTMPyP except for poly(rA)·poly(dT), in contrast to the large K values observed for poly(rA)·poly(rU) and poly(rA)·poly(dT). Thus, copper(II) insertion into the TMPyP chromophore leads to preferential binding to AT and AU base pairs rather than IC base pair although the number of binding sites is slightly limited.

CD Spectroscopy. As we pointed out previously (*35*), absorption spectroscopy may fail to detect a binding step if the associated spectral change is small. As an additional approach, we employed CD spectroscopy which is a sensitive probe of conformational change in nucleic acid duplexes. The CD spectral changes upon porphyrin binding are shown in Figure 3. In the case of poly(rA)·poly(rU), an isoelliptic point was seen at about 280 nm at concentrations of CuTMPyP below 10 μM, where the CD spectral change is small. The spectrum changed greatly upon addition of CuTMPyP, indicating that at least two binding processes are taking place and that drastic conformational changes in the duplex are occurring upon addition of the porphyrin. The spectral changes for the other duplexes were also drastic, although an isoelliptic point at about 250 nm was prominent in every case. The respective spectral changes were very similar to those observed for the binding of H_2TMPyP to the duplexes (*35*).

The changes in ellipticity were plotted against the concentration of CuTMPyP (Figure 4). The solid lines illustrate theoretical obtained using the K and n_{AB} values obtained from the absorbance data (Table 2). The theoretical curves for poly(rA)·poly(dT) and poly(rI)·poly(rC) are in good agreement with the observed changes in ellipticity. This indicates that binding proceeds in a single step and that the absorbance

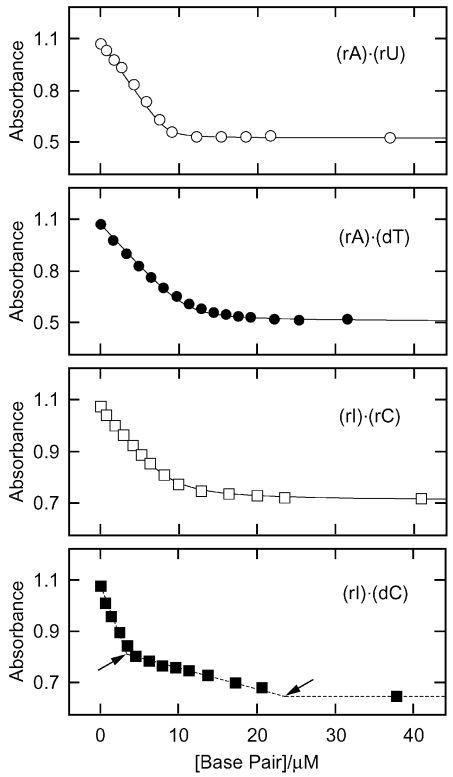

FIGURE 2: Absorbance change of CuTMPyP at 424 nm by the addition of duplexes. Open circles, poly(rA)·poly(rU); closed circles, poly(rA)·poly(dT); open squares, poly(rI)·poly(rC); closed squares, poly(rI)·poly(dC). Theoretical solid lines were drawn with the K and n_{AB} values in Table 2. Arrows indicate break points for the dashed line, which was drawn with the linear part of the absorbance change.

Table 2: Comparison of Binding Parameters between H_2TMPyP and CuTMPyP for the Duplexes

	CuTMPyP			H_2TMPyP[c]		
duplexes	$K/\mu M^{-1}$	n_{AB}[a]	n_{CD}[b]	$K/\mu M^{-1}$	n_{AB}[a]	n_{CD}[b]
poly(rA)·poly(rU)	18.5		0.32	0.68		0.30
		0.57	0.63		0.79	0.82
poly(rA)·poly(dT)	6.9	0.42	0.43	0.75	0.32	0.29
						0.69
poly(rI)·poly(rC)	2.6	0.55	0.51	8.5	0.65	0.65
poly(rI)·poly(dC)		0.19			0.25	
			0.54			0.59
		1.17			0.82	

[a] The n_{AB} values obtained from the absorbance changes. [b] The n_{CD} values obtained from the elliptic changes. [c] From ref 35.

and CD changes inform on the same binding process in both duplexes. In the case of poly(rA)·poly(rU), however, the observed ellipticity changes deviated considerably from the theoretical curve (Figure 4), and the CD changes describe a second binding step which is not detected by the absorbance changes (Figure 2). When two binding steps are distinct and can be treated separately, two n values are obtained independently from the break points (shown by arrows) of the dashed lines in Figure 4. The n values (n_{CD}) thus estimated are summarized in Table 2.

In the case of poly(rA)·poly(rU), the larger n value (n_{CD} = 0.63) was quite similar to that obtained from the absorbance change (n_{CD} = 0.57). Therefore, the n = 0.32 step for poly(rA)·poly(rU) is sensitive only to the conformational change of the duplexes. In the case of poly(rI)·poly(dC), the number of binding sites (n_{CD}) was evaluated from the break point of the ellipticity change (shown with an arrow in Figure 4), since the K and n_{AB} values could not be determined from the absorbance change. The value (n_{CD} = 0.54) coincided with neither of the n_{AB} values obtained from the absorbance changes (Table 2), and hence the conformational change in the poly(rI)·poly(dC) duplex does not parallel the electronic structural change of the porphyrin. The number of binding steps is quite similar for both CuTMPyP and H_2TMPyP (*35*), although a two step-binding of H_2TMPyP was observed for poly(rA)·poly(dT).

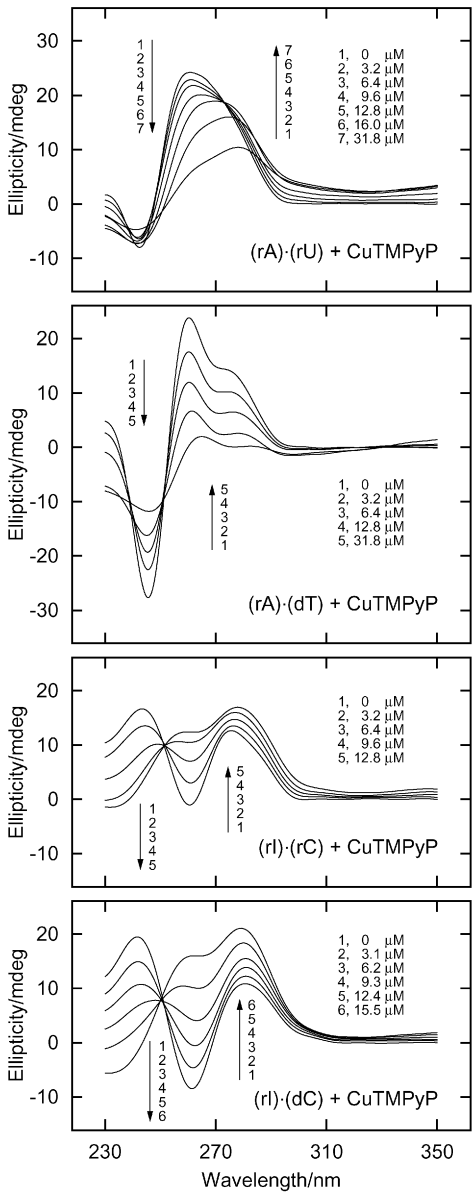

FIGURE 3: CD spectral changes of duplexes upon addition of CuTMPyP. The spectra were recorded in 10 mM sodium phosphate, 1 mM EDTA, 0.1 M NaCl (pH 7.0). Top: 32.3 μM poly(rA)·poly(rU). The concentrations of CuTMPyP: 1, 0 μM; 2, 3.2 μM; 3, 6.4 μM; 4, 9.6 μM; 5, 12.8 μM; 6, 16.0 μM; 7, 31.8 μM. Upper middle: 32.3 μM poly(rA)·poly(dT). The concentrations of CuTMPyP: 1, 0 μM; 2, 3.2 μM; 3, 6.4 μM; 4, 12.8 μM; 5, 31.8 μM. Lower middle: 32.3 μM poly(rI)·poly(rC). The concentrations of CuTMPyP: 1, 0 μM; 2, 3.2 μM; 3, 6.4 μM; 4, 9.6 μM; 5, 12.8 μM. Bottom: 32.3 μM poly(rI)·poly(dC). The concentrations of CuTMPyP: 1, 0 μM; 2, 3.1 μM; 3, 6.2 μM; 4, 9.3 μM; 5, 12.4 μM; 6, 15.5 μM.

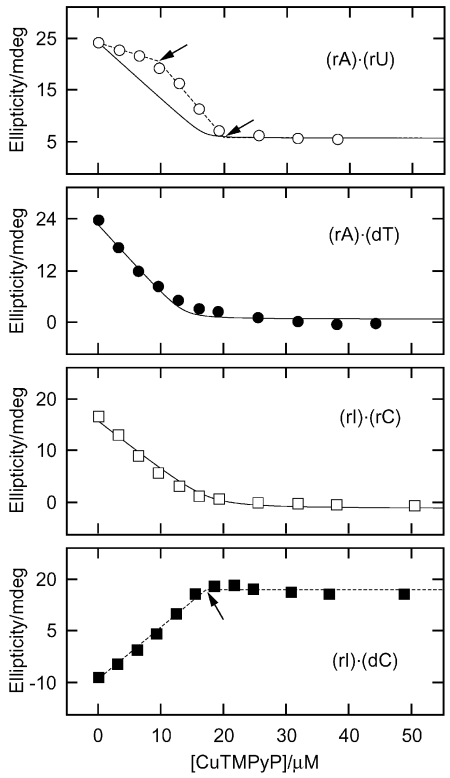

FIGURE 4: Changes in ellipticity of the duplexes upon addition of CuTMPyP. The base pair concentrations are given in Figure 3. Open circles, poly(rA)·poly(rU) at 262 nm; closed circles, poly(rA)·poly(dT) at 261 nm; open squares, poly(rI)·poly(rC) at 243 nm; closed squares, poly(rI)·poly(dC) at 262 nm. The solid lines were drawn with the K and n_{AB} values in Table 2. The dashed lines were drawn with the linear part of the ellipticity changes. The break points were marked with arrows.

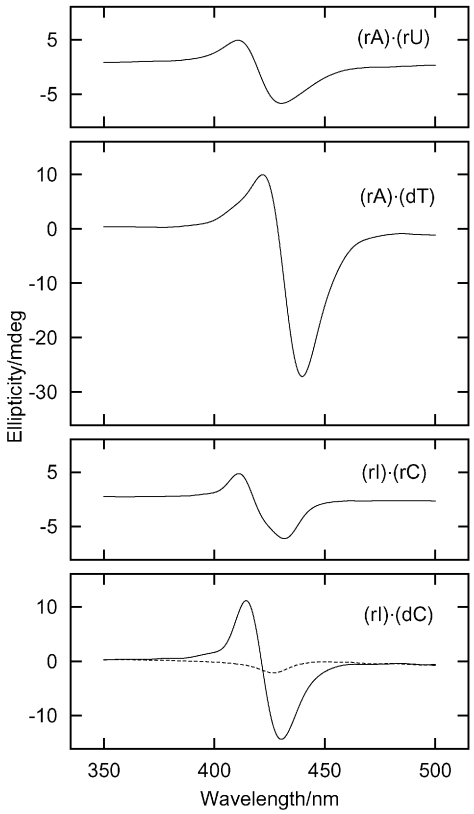

FIGURE 5: Induced CD spectra of CuTMPyP by the addition of duplexes. The porphyrin concentration was 4.66 μM for all duplexes. The spectra were recorded in 10 mM sodium phosphate, 1 mM EDTA, 0.1 M NaCl (pH 7.0). From top: 13.8 μM poly(rA)·poly(rU); 32.2 μM poly(rA)·poly(dT); 32.2 μM poly(rI)·poly(rC); 4.30 (solid line) and 51.4 (dashed line) μM poly(rI)·poly(dC).

Induced CD Spectroscopy. To clarify the binding modes of the porphyrin, the induced CD spectra (*9*, *12*) were measured at varying concentrations of the duplexes. As seen in Figure 5, conservative-type CD peaks were observed commonly for the duplexes, suggesting that the porphyrin binds externally with self-stacking along the polymer surface. In the case of poly(rA)·poly(rU), two-step binding was revealed by the ellipticity change (Figure 4), but the negative peak diminished only slightly at low duplex loads corresponding to the $n = 0.6$ step, perhaps indicating that the self-stacked porphyrin still dominates in this step. For poly(rI)·poly(dC), multiple binding steps were detected by the absorption and CD spectral changes (Figures 2 and 4), and hence we measured the induced CD spectra at lower loading ratios and higher amounts of the duplex (Figure 5). When the duplex concentration was low, strong conservative-type CD peaks were induced, whereas a negative CD peak was observed upon increasing the porphyrin concentration. Therefore, it is now clear that there are at least two modes of CuTMPyP binding to poly(rI)·poly(dC), self-stacking and intercalation. These binding features are shared by H_2TMPyP (*35*). A very strong bisignate spectrum of CuTMPyP is seen for poly(rA)·poly(dT) (Figure 5), but only negative CD was observed for H_2TMPyP (*35*). Thus, metal insertion changed the binding mode of the porphyrin for this polymer from intercalation to the self-stacking of the porphyrin.

Resonance Raman Spectroscopy. To reveal the structural changes in the CuTMPyP upon binding to the polymers, resonance Raman spectra were measured. Cumulative data for CuTMPyP bound to poly- and oligonucleotides reveal the porphyrin binding mode (*37*, *39*−*41*). Resonance Raman spectra of CuTMPyP bound to the duplexes are shown in Figure 6. For comparison, the spectra of free CuTMPyP (top) and poly[dG−dC]$_2$ bound porphyrin (bottom) are also shown. Although the spectral features are essentially the same, small but distinct frequency shifts were observed for some Raman lines. The sharp Raman line at 1367 cm^{-1} has been assigned to be ν_4 mode (*41*), which is mainly attributed to the pyrrole ν(N−Cα) symmetrical stretch. As ν_4 is essentially unshifted upon the addition of polymers, this line was used as an internal frequency standard to estimate the shift values of other bands. The shift values for the Raman lines are summarized in Figure 7. As reported previously, CuTMPyP intercalates into poly[dG−dC]$_2$ duplexes and the 1101 cm^{-1} line upshifts while the 1258 cm^{-1} line is downshifted (*39*, *40*). These lines have been assigned to δ(Cβ-H) and δ(Cm-pyr) bending modes, respectively (*41*). We observed similar frequency shift of these bands (ca. +4 cm^{-1} and −4 cm^{-1}, respectively). For poly(rA)·poly(rU), poly(rA)·poly(dT), poly(rI)·poly(rC), and poly(rI)·poly(dC) at low drug load (29.2 μM hybrid), these lines shifted similarly, although the shift values were relatively small (ca. +2 cm^{-1} and −2 cm^{-1}, respectively). Self-stacking of the CuTMPyP was revealed from the induced CD spectra for these polymers (Figure 5) except for poly(rI)·poly(dC), where intercalative binding was indicated at low drug loads. Thus, the pattern of shifts was almost identical for both self-stacking and intercalation, and hence the peripheral *N*-methylpyridyl moiety of CuTMPyP

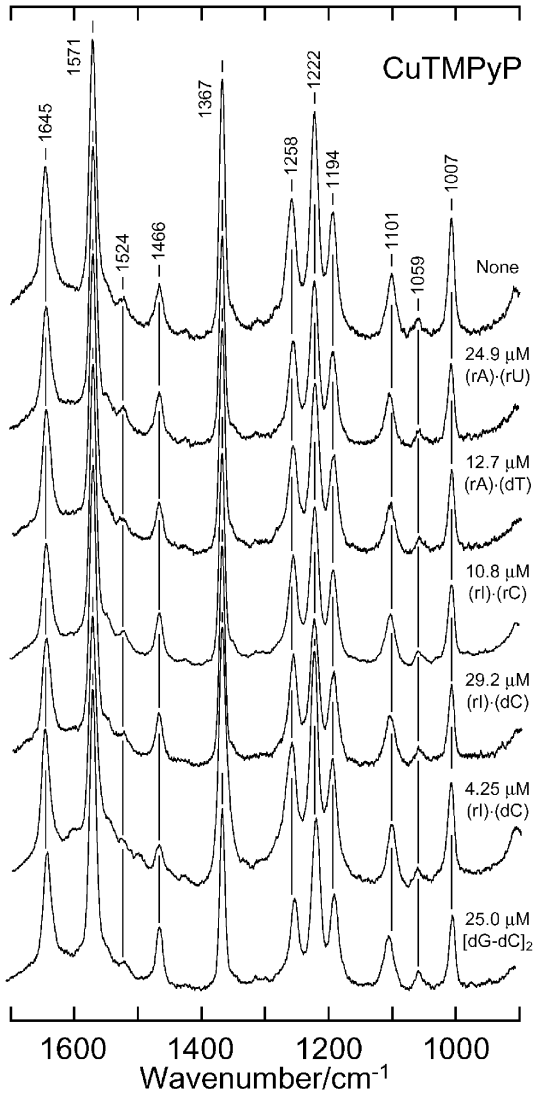

FIGURE 6: Resonance Raman spectra of CuTMPyP in the presence and absence of duplexes. The porphyrin concentration was 4.97 μM for all spectra. The samples were excited at 441.6 nm with laser power of 35 mW at the sample. The spectra were recorded in 10 mM sodium phosphate, 1 mM EDTA, 0.1 M NaCl (pH 7.0). From top: in the absence of duplexes; 24.9 μM poly(rA)·poly(rU); 12.7 μM poly(rA)·poly(dT); 10.8 μM poly(rI)·poly(rC); 29.2 μM poly(rI)·poly(dC); 4.25 μM poly(rI)·poly(dC); 25.0 μM poly[dG−dC]$_2$.

must have a common structure in both binding modes. In the presence of 4.25 μM poly(rI)·poly(dC), however, the shift is small, a feature which will be discussed later.

DISCUSSION

Binding Parameters. The binding parameters for CuTMPyP are compared with those for metal-free H_2TMPyP in Table 2. The n_{AB} values were obtained from the absorbance change at the Soret maximum, while the n_{CD} were obtained from the ellipticity changes. It is clear that the number of binding steps is conserved between two porphyrins, except for the binding to poly(rA)·poly(dT). In addition, the number of binding sites is generally small for CuTMPyP. This may imply that copper insertion diminishes the flexibility of the porphyrin skeleton, so that it is less able to adapt its conformation to the polymer surface. For

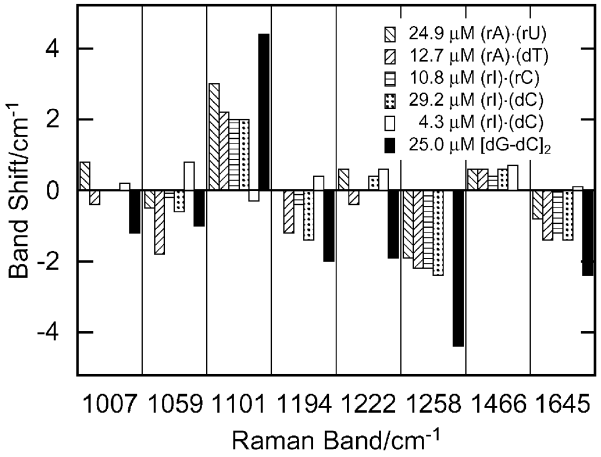

FIGURE 7: Frequency shift of the selected resonance Raman bands upon binding to the duplexes. From left for each line: 24.9 μM poly(rA)·poly(rU); 12.7 μM poly(rA)·poly(dT); 10.8 μM poly(rI)·poly(rC); 29.2 μM poly(rI)·poly(dC); 4.25 μM poly(rI)·poly(dC); 25.0 μM poly[dG−dC]$_2$.

poly(rI)·poly(dC), however, n_{AB} for the second step is very high. In this binding step, the porphyrin is stacked, as revealed by the induced CD spectrum (Figure 7). This suggests that the stacked porphyrins experience no sterical strain upon binding, and long helical alignment of the porphyrins is possible. This idea is supported by the resonance Raman spectrum of CuTMPyP in the presence of 4.25 μM poly(rI)·poly(dC). In this case, no frequency shifts in the Raman bands were apparent, and the spectrum was essentially the same with that of free CuTMPyP, indicating that the stacked porphyrin feels no strain on the polymer surface.

In Table 2, the binding constant, *K*, is compared between the porphyrins. It is striking that the *K* value for poly(rA)·poly(rU) is increased more than 25-fold by copper insertion. This polymer accommodates CuTMPyP in two steps, and the *K* value corresponds to the step with the larger *n* value. The first step was detected only by CD spectroscopy (Figure 4), suggesting that the absorption spectrum of CuTMPyP is indistinguishable between the first and second steps. Although the *K* value for the first step could not be determined for reasons which are complex, the first step must have a higher binding constant than that for the second step, and the favorable binding of CuTMPyP to the poly(rA)·poly(rU) is strongly suggested.

For the binding to poly(rA)·poly(dT), the *K* value also increased by about 10-fold (Table 2), and the binding mode changed from intercalation (H_2TMPyP) to self-stacking (CuTMPyP) as revealed by the induced CD spectra (Figure 5). For poly(rI)·poly(rC), the *K* value for H_2TMPyP decreased by a factor of 3 upon copper insertion. Thus, we may conclude that the copper directs the TMPyP chromophore to rA·rU and rA·dT sequences in preference to rI·rC and rI·dC sequences. Recently, binding of various drugs to hybrids, including poly(rA)·poly(rU) and poly(rA)·poly(dT), was examined by equilibrium dialysis methods (*34*). It was reported that among the 84 drugs tested which included H_2TMPyP, ellipticine has the highest affinity ($K = 0.44$ μM^{-1}) for poly(rA)·poly(dT). Direct comparison of these data with those presented here is complicated by the different solution conditions, but we can conclude that copper insertion

is a viable way to enhance the affinity of TMPyP for RNA and hybrid duplexes having AT and AU base pairs.

Spectroscopic Characteristics. The structural basis of the large increase of CuTMPyP affinity has been probed by various spectroscopic methods. In Table 1, a comparion between the spectral properties of H_2TMPyP and CuTMPyP is summarized. The bathochromic shift ($\Delta\lambda$) and hypochromicity are consistently small for CuTMPyP, and this suggests that the porphyrin π-electrons are less perturbed in CuTMPyP. Recent theoretical studies suggest that nonplanar porphyrins show red-shifted electronic spectra (*42*). In accord with this, the positive and negative peaks in the induced CD spectra are always about 10 nm blue-shifted for the CuTMPyP, suggesting a more planar porphyrin macrocycle structure. In the case of poly(rA)·poly(dT), the binding mode is changed by copper insertion, and it seems reasonable that a planar structure would be more suitable for self-stacking. The signal intensities of the induced CD peaks are shown in Figure S1. As we reported previously (*35*), the intensity correlated almost linearly with the *n* value for H_2TMPyP (dashed lines), and we have found a similar correlation for CuTMPyP. The slope is steeper for CuTMPyP, suggesting that CuTMPyP is more ordered on the polymer surface than H_2TMPyP. Collectively, the copper maintains a flat porphyrin core so that stacking is made easy. It is clear, however, that the signal intensities for CuTMPyP are greatly enhanced upon binding to poly(rA)·poly(dT) (Table 1), suggesting that this polymer has a special structure, as will be discussed later.

The structural changes in the porphyrin are revealed by resonance Raman spectroscopy. It has been reported that the upshift of the 1101 cm^{-1} line and the downshift of the 1258 cm^{-1} line signify intercalation of the porphyrin core (*39*, *40*). In accord with this, we were able to observe approximately +4 and −4 cm^{-1} shifts in these lines upon binding to poly-[dG−dC]$_2$. From the negative induced CD peak, we infer intercalation into poly(rI)·poly(dC) at low drug loads (Figure 5, dashed line). Under these conditions (29.2 μM hybrid), we observed relatively small ca. +2 and −2 cm^{-1} shifts of the intercalation markers. This must indicate that the porphyrin periphery experiences less strain upon intercalation into rI·dC than its does upon intercalation into dG·dC base pairs. Upon intercalation, the methylpyridyl ring is inclined toward the porphyrin plane (*12*), which induces a clash between the pyrrole Cβ-H and the *ortho*-hydrogen of the pyridyl moieties (*40*). Inosine bases lack the 2-amino group and the IC base pair has a smaller area than the GC pair, so that less steric strain will be exerted on the intercalated CuTMPyP.

For the other duplexes, CuTMPyP was found to self-stack on the polymer surface (Figure 5), and the Raman markers show similar frequency shifts to those for intercalation into poly(rI)·poly(dC). Thus, the shift patterns for the intercalated and self-stacked porphyrins are quite similar, indicating that the porphyrin structure is little changed between these binding modes. However, for poly(rI)·poly(dC) at high drug load (4.25 μM hybrid), the frequencies of the Raman lines are almost identical to those of free CuTMPyP, and long-range alignment of the porphyrins may be allowed, as discussed above. With this in mind, the frequency shifts seem to be correlated with the *n* values. Namely, the shift values for the stacked CuTMPyP decreases in the order: poly(rA)·poly(rU) (n_{AB} = 0.32), poly(rA)·poly(dT) (n_{AB} = 0.42), poly(rI)·poly(rC) (n_{AB} = 0.46), poly(rI)·poly(dC) (n_{AB} = 1.17). Thus, large *n* values are allowed when the steric strain exerted on the porphyrin periphery is small. In other words, the helical flexibility of the duplexes may allow the porphyrin to align with less rotation of its periphery.

Anomaly of poly(rA)·poly(dT). In the presence of large amounts of RNA duplex, H_2TMPyP preferred self-stacking on the polymer surface (*35*), and this binding mode was conserved for CuTMPyP. This can be understood in terms of the structure of the RNA duplex. In the canonical RNA duplex, the furanose rings are puckered C3′-*endo*, with the base pairs displaced from the helical axis. This results in a wide and shallow minor groove, allowing the porphyrin to stack easily on the surface in an ordered manner. Since copper insertion flattens the porphyrin and facilitates stacking, this binding mode can be maintained. On the other hand, H_2TMPyP prefers the intercalative mode of binding to hybrids (*35*). This is also true for CuTMPyP binding to poly(rI)·poly(dC) at low drug load, as revealed by the induced CD spectra (Figure 5). However, as discussed above, binding to poly(rA)·poly(dT) hybrid led to (a) a change in the binding mode following copper insertion; (b) strong induced CD peaks; and (c) induced CD peaks red-shifted by about 10 nm. The anomaly of poly(rA)·poly(dT) must be attributable to its unique structure among the hybrids.

It has been proposed that the higher the percentage of purine on the RNA strand, the closer the hybrid duplex is to the A-form (*43*). In accord with this, X-ray fiber diffraction showed that poly(rI)·poly(dC) adopted a regular A-form conformation (C3′-*endo*) (*44*). A notable exception (*45*) is poly(rA)·poly(dT), which was found to have C2′-*endo* DNA sugar puckers (*46*). This bimorphic "hybrid" structure is also supported by Raman (*47*) and NMR (*48*) studies. In the proposed model, the poly(dT) strand sugars adopt the C2′-*endo* pucker as seen in B-form DNA; thus, the bases are situated close to the helix axis (*46*, *47*). This inward displacement ought to allow CuTMPyP to stack close to this axis. Although the structural details of stacked porphyrins are not clear at present, it should be noted that close location of a chromophore to the helical axis has been shown theoretically to be associated with large induced CD signals (*49*). Thus, the porphyrin moiety could be a sensitive probe for helical structures of polynucleotides.

CONCLUSION

As discussed above, copper insertion has been shown to confer unique characteristics on the cationic TMPyP, and this was attributed to a flattening of the porphyrin core, leading to self-stacking of this chromophore on the polymer surface. The porphyrin-polymer interaction is governed by many factors, and the helical structure of the polymers is sequence-dependent. Thus, simple modifications of the porphyrin, such as copper insertion, can result in drastic increases in its affinity for specific polynucleotides. Our approach will provide an easy way to improve the efficiency of porphyrins in medical applications, targeting polynucleotides in malignant cells.

ACKNOWLEDGMENT

The authors thank Dr. Anthony J. Wilkinson, University of York, U.K., for valuable discussion.

SUPPORTING INFORMATION AVAILABLE

Figure S1 showing linear correlation between the number of binding sites (*n*) and the molar ellipticities of the porphyrin induced CD peaks. This material is available free of charge via the Internet at http://pubs.acs.org.

REFERENCES

1. Dougherty, T. J. (1993) *Photochem. Photobiol. 58*, 895.
2. Villanueva, A., Juarranz, A., Diaz, V., Gomez, J., and Canete, M. (1992) *Anticancer Drug Des. 7*, 297.
3. Verlhac, J. B., Gaudemer, A., and Kraljic, I. (1983) *Nouv. J. Chim. 8*, 401.
4. Ishikawa, Y., Yamakawa, N., and Uno, T. (2002) *Bioorg. Med. Chem. 10*, 1953.
5. Fiel, R. J. (1989) *J. Biomol. Struct. Dyn. 6*, 1259.
6. Pasternack, R. F., and Gibbs, E. J. (1989) *ACS Symp. Ser. 402*, 59.
7. Marzilli, L. G. (1990) *New J. Chem. 14*, 409.
8. Pasternack, R. F., Gibbs, E. J., and Villafranca, J. J. (1983) *Biochemistry 22*, 5409.
9. Pasternack, R. F., Garrity, P., Ehrlich, B., Davis, C. B., Gibbs, E. J., Orloff, G., Giartosio, A., and Turano, C. (1986) *Nucleic Acids Res. 14*, 5919.
10. Pasternack, R. F., Giannetto, A., Pagano, P., and Gibbs, E. J. (1991) *J. Am. Chem. Soc. 113*, 7799.
11. Pasternack, R. F., Bustamante, C., Collings, P. J., Giannetto, A., and Gibbs, E. J. (1993) *J. Am. Chem. Soc. 115*, 5393.
12. Pasternack. R. F., Gibbs, E. J., and Villafranca, J. J. (1983) *Biochemistry 22*, 2406.
13. Pasternack, R. F., Brigandi, R. A., Abrams, M. J., Williams, A. P., and Gibbs, E. J. (1990) *Inorg. Chem. 29*, 4483.
14. Perry, P. J., and Jenkins, T. C. (1999) *Expert Opin. Investig. Drugs 8*, 1981.
15. Han, H., and Hurley, L. H. (2000) *Trends Pharmacol. Sci. 21*, 136.
16. Anantha, N. V., Azam, M., and Sheardy, R. D. (1998) *Biochemistry 37*, 2709.
17. Salazar, M., Thompson, B. D., Kerwin, S. M., and Hurley, L. H. (1996) *Biochemistry 35*, 16110.
18. Sun, D., Thompson, B., Cathers, B. E., Salazar, M., Kerwin, S. M., Trent, J. O., Jenkins, T. C., Neidle, S., and Hurley, L. H. (1997) *J. Med. Chem. 40*, 2113.
19. Wheelhouse, R. T., Sun, D., Han, H., Han. F. X., and Hurley, L. H. (1998) *J. Am. Chem. Soc. 120*, 3261.
20. Haq, I., Trent, J. O., Chowdhry, B. Z., Jenkins, T. C. (1999) *J. Am. Chem. Soc. 121*, 1768.
21. Blackburn, E. H. (1991) *Nature 350*, 569.
22. Kang, C. H., Zhang, X., Ratliff, R., Moyzis, R., and Rich, A. (1992) *Nature 356*, 126.
23. Wellinger, R. J., and Sen, D. (1997) *Eur. J. Cancer 33*, 735.
24. Lundblad, V., and Wright, W. E. (1996) *Cell 87*, 369.
25. Kim, N. W., Piatyszek, A. M., Prowse, K. R., Harley, C. B., West, M. D., Ho, P. L. C., Coviello, G. M., Wright, W. E., Weinrich, S. L., and Shay, J. W. (1994) *Science 266*, 2011.
26. Guliaev, A. B., and Leontis, N. B. (1999) *Biochemistry 38*, 15425.
27. Celander, D. W., and Nussbaum, J. M. (1996) *Biochemistry 35*, 12061.
28. Pratt, W. R., Ruddon, R., Ensminger, W. D., and Maybaum, J. (1994) *The Anticancer Drugs*, Vol. 2, p 306, Oxford University Press, Oxford.
29. Mathews, C. K., van Holde, K. E., and Ahern, K. G. (2000) *Biochemistry*, Vol. 3, p 876ff, Benjamin/Cummings, San Francisco.
30. McEachern, M. J., Krauskopf, A., and Blackburn, E. H. (2000) *Annu. Rev. Genet. 34*, 331.
31. Glukhov, A. I., Zimnik, O. V., Gordeev, S. A., and Severin, S. E. (1998) *Biochem. Biophys. Res. Commun. 248*, 368.
32. Gmeiner, W. H., Cui, W., Konerding, D. E., Keifer, P. A., Sharma, S. K., Soto, A. M., Marky, L. A., and Lown, J. W. (1999) *J. Biomol. Struct. Dyn. 17*, 507.
33. Gmeiner, W. H., Cui, W., Sharma, S., Soto, A. M., Marky, L. A., and Lown, J. W. (2000) *Nucleosides, Nucleotides, Nucleic Acids 19*, 1365.
34. Ren, J., Qu, X., Dattagupta, N., and Chaires, J. B. (2001) *J. Am. Chem. Soc. 123*, 6742.
35. Uno, T., Hamasaki, K., Tanigawa, M., and Shimabayashi, S. (1997) *Inorg. Chem. 36*, 1676.
36. Pasternack, R. F., Francesconi, L., Raff, D., and Spiro, E. (1973) *Inorg. Chem. 12*, 4327.
37. Bütje, K., and Nakamoto, K. (1990) *Inorg. Chim. Acta 167*, 97.
38. Correia, J. J., and Chaires, J. B. (1994) *Methods Enzymol. 240*, 593.
39. Bütje, K., and Nakamoto, K. (1990) *J. Inorg. Biochem. 39*, 75.
40. Bütje, K., Schneider, J. H., Kim, J.-J. P., Wang, Y., Ikuta, S., and Nakamoto, K. (1989) *J. Inorg. Biochem. 37*, 119.
41. Blom, N., Odo, J., Nakamoto, K., and Strommen, D. P. (1986) *J. Phys. Chem. 90*, 2847.
42. Parusel, A. B. J., Wondimagegn, T., and Ghosh, A. (2000) *J. Am. Chem. Soc. 122*, 6371.
43. Xiong, Y., and Sundaralingam, M. (1998) *Structure 6*, 1493.
44. Arnott, S., Chandrasekaran, R., Millane, R. P., and Park, H.-S. (1986) *J. Mol. Biol. 188*, 631.
45. Saenger, W. (1984) *Principles of Nucleic Acid Structure*, pp. 280−281, Springer-Verlag, New York.
46. Zimmerman, S. B., and Pheiffer, B. H. (1981) *Proc. Natl. Acad. Sci. U.S.A. 78*, 78.
47. Benevides, J. M., and Thomas, G. J., Jr. (1988) *Biochemistry 27*, 3868.
48. Shindo, H., and Matsumoto, U. (1984) *J. Biol. Chem. 259*, 8682.
49. Kubista, M., Åkerman, B., and Nordén, B. (1988) *J. Phys. Chem. 92*, 2352.

BI026139Z